Smart Structures and Systems, *Vol. 27, No. 6 (2021) 891-901*
DOI: https://doi.org/10.12989/sss.2021.27.6.891

Active structural acoustic control using an integrated control system with smart structures

Huaifeng Cui*[1], Rufu Hu [1a] and Nan Chen [2b]

[1] *School of Mechanical Engineering, Ningbo University of Technology, Ningbo 315211, Zhejiang, China*
[2] *School of Mechanical Engineering, Southeast University, Nanjing 211189, Jiangsu, China*

(*Received February 13, 2019, Revised November 17, 2020, Accepted April 3, 2021*)

Abstract. An integrated control system with smart structure is proposed for active structural acoustic control (ASAC). It is mainly used to integrate the advantages of centralized and decentralized ASAC. Each smart structure contains a relatively independent controller, which forms a distributed control. The coordination and cooperation between smart structures is mainly realized by sending control factors (secondary generalized modal force) from the upper coordination unit (coordination structure) to each smart structure. The control factor can reflect the weight of each smart structure on vibration noise control, and play a key role in noise control. The control factors are extracted from the blend function in the bottom control units (smart structures) and stored in the coordination structure. This design method ensures the consistency of the internal functions of each smart structure and lays a foundation for decentralized control. In addition, whether the control factor is allocated to the smart structure depends on the real-time changes of the sound field. Through the intelligent allocation of the control factors, the global (centralized) control is realized and the coupling problem between smart structures is solved. Since the control system does not have a centralized controller, it appears as a decentralized control in form; at the same time, the centralized control in algorithm is achieved by extracting and redistributing the control factors. Therefore, the control system integrates the advantages of decentralized and centralized control.

Keywords: integrated control; decentralized and centralized control; smart structure; active structural acoustic control; enclosure; control factor

1. Introduction

Active structural acoustic control (ASAC) is an active control technique that attenuates noise by suppressing structural vibration. Compared with active noise control, the ASAC is more difficult to popularize in practice. It is partly due to the low reliability, and difficult installation and maintenance of the ASAC system (Aridogan and Basdogan 2015). The ASAC has distributed characteristics, and its control methods mainly include centralized, decentralized and distributed control. Frampton *et al*. (2010) elaborated on these control methods and compared their control performances. The centralized vibro-acoustic control enables global optimization and high control performance, but it lacks the advantages of decentralized vibro-acoustic control, such as high reliability, easy implementation and scalability. Some researchers have studied the decentralized vibro-acoustic control (Gardonio *et al*. 2004a, b, Alujevi *et al*. 2008, Engels *et al*. 2006, Engels and Elliott 2008), and the results show that its control performance can reach the level of centralized control only under certain conditions (Frampton *et al*. 2010). The main advantage of the decentralized control is its reduced complexity, ease of implementation, and robustness to individual control unit failure and so on (Quaegebeur *et al*. 2009, Yuan *et al*. 2015). The goal of distributed control is to explore how to integrate the advantages of centralized and decentralized control (Baumann and Elliott 2007, Frampton 2006). Frampton (2006) investigated various architectures for the distributed structural acoustic control and indicated that distributed control performs better than decentralized control. However, it is inferior to the performance of centralized control.

Some researchers have applied smart structures to the study of ASAC (Ringwelski and Gabbert 2010, Bagha and Modak 2017). Ringwelski and Gabbert (2010) used the velocity feedback control algorithm to design a closed-loop model of the ASAC with smart structure. The genetic algorithms are applied to the smart structure which consisted of a supporting core isotropic layer perfectly bonded to lower/upper piezoelectric sensor/actuator skin layers (Hasheminejad and Shakeri 2017). The multi-objective particle swarm optimization control system in combination with the passive action of the carbon fiber–reinforced polymer is expected to be applied to smart structure design in the future (Hasheminejad *et al*. 2018). Larbi *et al*. (2012) presented the finite element implementation of vibroacoustic problems with piezoelectric composite structures connected to electric shunt circuits. The smart property of the smart structures mentioned above is mainly reflected in the structure itself rather than in the control algorithm.

*Corresponding author, Ph.D.,
E-mail: cuihuaifeng@126.com

ISSN: 1738-1584 (Print), 1738-1991 (Online)

The control architectures of decentralized and distributed vibro-acoustic control are almost single mode. Whether or not the noise standard is met, the control units in the system are normally activated at execution time. It is necessary to design a control architecture in the ASAC to enable the control unit to start or stop according to the changes of the external environment, in order to achieve the purpose of adjusting control mode and saving resources.

Through long-term practice, it is found that the problem of the ASAC of a complex system must be solved by high dimensional coupled system. However, fully continuous distributed control mechanisms are used for complex large-scale systems, if not impossible, it is also expensive. Therefore, it is necessary to study more reasonable control framework. The limited discrete distribution control of the control unit is definitely one of the solutions, but this results in the coordination problem between the control units (Algermissen and Monner 2017, Schiller and Cabell 2010). Due to the complexity of the high dimensional coupled system, the random disturbance has a great influence on the stability and reliability of the system (Landau *et al*. 2011), thus it is needed to adopt an intelligent method.

In this paper, an integrated control method based on smart structure is proposed for the ASAC. According to the characteristics of the coupled sound field in the enclosure with multi-elastic wall, the global control problem is decomposed into several local control problems. The local control problem is solved by smart structure. The smart structure includes the sensors, actuator, and intelligent controller. It can start or stop according to the change of the external environment. The global control problem is solved by the joint control of the smart structures. The cooperation between the smart structures is achieved using a coordination structure. The control factor, namely the generalized mode secondary force, is extracted from the bottom control unit (smart structure) into the upper organization (coordination structure), and then allocated to each smart structure according to the real-time change of the sound field. The contribution of the smart structure to noise suppression is largely reflected in the control factor. This design method realizes centralized control and solves the coupling problem between the smart structures. The smart structure of modular design is actually a complete sub-control system. This makes the system feature of decentralized control. Therefore, the decentralized control and centralized control are integrated to form an integrated control system.

2. Coupled sound field modeling

2.1 Theoretical formulation

Fig. 1 shows panel-cavity system that is modeled in this analysis. Consider a rectangular enclosure that has two simply supported flexible panels and four rigid boundaries. The two flexible panels are labeled as Panel *a* and Panel *b*, and located at $z = L_z$ and $y = L_y$, respectively. These panels are assumed to be thin and isotropic. The dimensions of the enclosure are $L_x \times L_y \times L_z = 0.868$ m × 1.15 m × 1 m. A sinusoidal excitation force F is imposed on the Panel *a*,

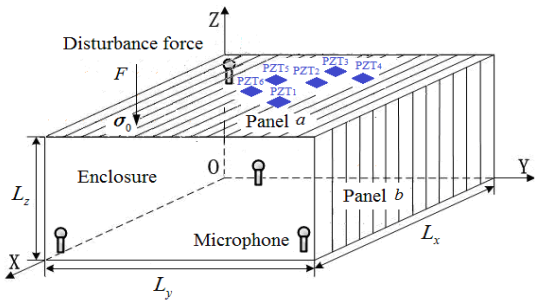

Fig. 1 Acoustic cavity model with two elastic panels

which, in turn, radiates sound power into the cavity. Six patches of lead zirconate titanate (PZT) piezoelectric patches are also bound to the outer surface of Panel *a* to form actuators, and all the patches are assumed to have the same geometrical and material characteristics. Four microphones in the enclosure serve as sensors.

With the system described above, the acoustic pressure in the enclosure is governed by the inhomogeneous wave equation as

$$\nabla^2 p(\boldsymbol{r},t) - \frac{1}{c^2}\frac{\partial^2 p(\boldsymbol{r},t)}{\partial t^2} = \rho\frac{\partial^2 w_a}{\partial t^2}\delta(z-L_z) + \rho\frac{\partial^2 w_b}{\partial t^2}\delta(y-L_y) \tag{1}$$

Where $p(\boldsymbol{r}, t)$ is the sound pressure, $\boldsymbol{r}$ represents the coordinate of any point in the enclosure, t represents time variable, ∇^2 is the Laplacian operator. c is the sound speed, and ρ is the mass density of air. w_a and w_b are the displacements of the panels *a* and *b*, respectively. $\delta(.)$ is one-dimensional Dirac delta function of a coordinate normal to the surface.

The equations of motion of panels *a* and *b* can be expressed as

$$\rho_a h_a \ddot{w}_a + D_a\nabla^4 w_a = F\delta(\boldsymbol{\sigma}_a - \boldsymbol{\sigma}_0) + \sum_k \left[\frac{(h_a+h_p)E_{\text{pzt}}d_{31}}{(1-\nu_p)}\right](\nabla^2\chi_k)V_k(t) - p(\boldsymbol{\sigma}_a,t) \tag{2}$$

$$\rho_b h_b \ddot{w}_b + D_b\nabla^4 w_b = -p(\boldsymbol{\sigma}_b,t) \tag{3}$$

Where ρ_a, h_a, D_a and ρ_b, h_b, D_b are the material density, thickness, and bending stiffness of panels *a* and *b*, respectively. $\nabla^4 = \nabla^2\nabla^2$, $D_a = \frac{E_a h_a^3}{12(1-\nu_a)}$, $D_b = \frac{E_b h_b^3}{12(1-\nu_b)}$, here, E_a, ν_a and E_b, ν_b represent Young's modulus and Poisson's ratio of panels *a* and *b*, respectively. The terms $p(\boldsymbol{\sigma}_a, t)$ and $p(\boldsymbol{\sigma}_b, t)$ are the acoustic pressure on the inner surface of panels *a* and *b*, respectively. $\boldsymbol{\sigma}_a = (x, y, L_z)$ and $\boldsymbol{\sigma}_b = (x, L_y, z)$ denote the coordinate on the surface of panels *a* and *b*, respectively. $\boldsymbol{\sigma}_0$ is the coordinate of disturbance force F on the surface of Panel *a*. $\delta(.)$ is the two-dimensional Dirac function. h_p, E_{pzt}, ν_p and d_{31} represent the thickness, Young's modulus, Poisson's ratio and dielectric constant of PZT patches, respectively. The function χ_k is unity, where the kth PZT patches exist and is zero otherwise, and k is the number of PZT patches. $V_k(t)$ is the control voltage applied

to the *k*th PZT patch.

If the acoustic pressure in the enclosure and the structural vibration of panels *a* and *b* are assumed to be described by the summation of *N*, *M* and *S* modes, respectively, the acoustic pressure and the normal structural vibration velocities of panels *a* and *b* are given, respectively, by

$$p(\boldsymbol{r},t)=\sum_{n=1}^{N}\psi_n(\boldsymbol{r})P_n(t) \tag{4}$$

$$u_a(\boldsymbol{\sigma}_a,t)=\sum_{m=1}^{M}\varphi_m(\boldsymbol{\sigma}_a)\,V_{am}(t) \tag{5}$$

$$u_b(\boldsymbol{\sigma}_b,t)=\sum_{s=1}^{S}\varphi_s(\boldsymbol{\sigma}_b)\,V_{bs}(t) \tag{6}$$

Where $\psi_n(r)=\cos(n_1\pi x/L_x)\cos(n_2\pi y/L_y)\cos(n_3\pi z/L_z)$ is the uncoupled acoustic mode shape function, (n_1, n_2, n_3) are the modal indices of the *n*th cavity mode. $\varphi_m(\sigma_a)=\sin(m_1\pi x/L_x)\sin(m_2\pi y/L_y)$ and $\varphi_s(\sigma_b)=\sin(s_1\pi x/L_x)\sin(s_2\pi z/L_z)$ are the uncoupled structural mode shape functions of panels *a* and *b*, respectively, (m_1, m_2) are the modal indices of the *m*th mode of the Panel *a*, (s_1, s_2) are the modal indices of the *s*th mode of the Panel *b*. $P_n(t)$, $V_{am}(t)$ and $V_{bs}(t)$ are time-dependent modal amplitudes to be determined. Due to the orthogonal properties of the uncoupled acoustic and structural mode shape functions, we have

$$M_n=\int_V\psi_n(r)\,\psi_n(r)dV \tag{7}$$

$$M_{am}=\rho_a h_a\int_{A_a}\varphi_m(\sigma_a)\,\varphi_m(\sigma_a)dA \tag{8}$$

$$M_{bs}=\rho_b h_b\int_{A_b}\varphi_s(\sigma_b)\,\varphi_s(\sigma_b)dA \tag{9}$$

Where M_n is the *n*th acoustic modal mass, M_{am} is the *m*th structural modal mass of Panel *a*, and M_{bs} is the *s*th structural modal mass of Panel *b*. A_a and A_b are the areas of panels *a* and *b*, respectively. Considering the case for a harmonic external disturbance with frequency ω, utilizing Eqs. (4)-(9) and taking into account the modal damping terms, the following equations for the structural-acoustic coupled system can be derived from Eqs. (1)-(3) by Fourier transform

$$\ddot{P}_n(\omega)+2\xi_n\omega_n\dot{P}_n(\omega)+\omega_n^2P_n(\omega)=\frac{j\omega\rho c^2}{M_n}\left(A_a\sum_{m=1}^{M}C_{nm}^a\,V_{am}(\omega)+A_b\sum_{s=1}^{S}C_{ns}^b\,V_{bs}(\omega)\right) \tag{10}$$

$$\ddot{V}_{am}(\omega)+2\xi_{am}\omega_{am}\dot{V}_{am}(\omega)+\omega_{am}^2V_{am}(\omega)=\frac{j\omega}{M_{am}}\left(Q_{Fm}+\sum_k D_{m,k}V_k-A_a\sum_{n=1}^{N}C_{nm}^a\,P_n(\omega)\right) \tag{11}$$

$$\ddot{V}_{bs}(\omega)+2\xi_{bs}\omega_{bs}\dot{V}_{bs}(\omega)+\omega_{bs}^2V_{bs}(\omega)=\frac{j\omega}{M_{bs}}\left(-A_b\sum_{n=1}^{N}C_{ns}^b\,P_n(\omega)\right) \tag{12}$$

Where ω_n, ω_{am} and ω_{bs} are natural frequencies of uncoupled cavity and panels, ξ_n, ξ_{am} and ξ_{bs} are modal damping ratios of fluid and panels, respectively. C_{nm}^a and C_{ns}^b given by $C_{nm}^a=\frac{1}{A_a}\int_{A_a}\psi_n(z=L_z)\varphi_m(\sigma_a)\,dA$ and $C_{ns}^b=\frac{1}{A_b}\int_{A_b}\psi_n(y=L_y)\varphi_s(\sigma_b)dA$, respectively, are dimensionless modal coupling coefficients. Q_{Fm} and $D_{m,k}$ given by $Q_{Fm}=\int_{A_a}F\delta(\sigma-\sigma_0)\,\varphi_m(\sigma_a)dA$ and $D_{m,k}=\frac{(h_a+h_p)E_{\mathrm{pzt}}d_{31}}{(1-v_p)}\int_{A_a}\varphi_m(\sigma_a)\,(\nabla^2\chi_k)dA$ are defined as primary and secondary generalized modal forces.

The following equations can be drawn from Eqs. (10)-(12) and written as

$$P_n(\omega)=\frac{h_n\rho c^2}{M_n}\left(A_a\sum_{m=1}^{M}C_{nm}^a\,V_{am}(\omega)+A_b\sum_{s=1}^{S}C_{ns}^b\,V_{bs}(\omega)\right) \tag{13}$$

$$V_{am}(\omega)=\frac{h_{am}}{M_{am}}\left(Q_{Fm}(\omega)+\sum_k D_{m,k}V_k-A_a\sum_{n=1}^{N}C_{nm}^a\,P_n(\omega)\right) \tag{14}$$

$$V_{bs}(\omega)=\frac{h_{bs}}{M_{bs}}\left(-A_b\sum_{n=1}^{N}C_{ns}^b\,P_n(\omega)\right) \tag{15}$$

Where

$$h_n(\omega)=\begin{cases}1/(1/T_a+j\omega), & \text{when}\quad n=1\\ j\omega/(\omega_n^2+2j\xi_n\omega_n\omega-\omega^2), & \text{when}\quad n\neq 1\end{cases},$$

here T_a is the time constant of the first mode, $h_{am}=\frac{j\omega}{\omega_{am}^2+2j\xi_{am}\omega_{am}\omega-\omega^2}$, $h_{bs}=\frac{j\omega}{\omega_{bs}^2+2j\xi_{bs}\omega_{bs}\omega-\omega^2}$.

We can express Eqs. (13)-(15) in the form of matrices and complex amplitude vectors

$$\boldsymbol{P}=\boldsymbol{Z}_a\boldsymbol{V}_a+\boldsymbol{Z}_b\boldsymbol{V}_b \tag{16}$$

$$\boldsymbol{V}_a=\boldsymbol{Q}_F+\boldsymbol{D}_k\boldsymbol{V}-\boldsymbol{H}_a\boldsymbol{P} \tag{17}$$

$$\boldsymbol{V}_b=-\boldsymbol{H}_b\boldsymbol{P} \tag{18}$$

Here are the specific expressions of some parameter vectors

$$\boldsymbol{Z}_a=\left[\frac{h_1\rho c^2A_a\boldsymbol{C}_1^a}{M_1}\quad\frac{h_2\rho c^2A_a\boldsymbol{C}_2^a}{M_2}\quad\ldots\quad\frac{h_n\rho c^2A_a\boldsymbol{C}_n^a}{M_n}\right]^T \tag{19}$$

$$\boldsymbol{Z}_b=\left[\frac{h_1\rho c^2A_b\boldsymbol{C}_1^b}{M_1}\quad\frac{h_2\rho c^2A_b\boldsymbol{C}_2^b}{M_2}\quad\ldots\quad\frac{h_n\rho c^2A_b\boldsymbol{C}_n^b}{M_n}\right]^T \tag{20}$$

$$\boldsymbol{Q}_F = \left[\frac{h_{a1}Q_{F1}}{M_{a1}} \quad \frac{h_{a2}Q_{F2}}{M_{a2}} \quad \cdots \quad \frac{h_{am}Q_{Fm}}{M_{am}}\right]^T \tag{21}$$

$$\boldsymbol{D}_k = \begin{bmatrix} \frac{h_{a1}D_{1,1}}{M_{a1}} & \frac{h_{a1}D_{1,2}}{M_{a1}} & \cdots & \frac{h_{a1}D_{1,k}}{M_{a1}} \\ \frac{h_{a2}D_{2,1}}{M_{a2}} & \frac{h_{a2}D_{2,2}}{M_{a2}} & \cdots & \frac{h_{a2}D_{2,k}}{M_{a2}} \\ \vdots & \vdots & \ddots & \vdots \\ \frac{h_{am}D_{m,1}}{M_{am}} & \frac{h_{am}D_{m,2}}{M_{am}} & \cdots & \frac{h_{am}D_{m,k}}{M_{am}} \end{bmatrix} \tag{22}$$

$$\boldsymbol{H}_a = \left[\frac{h_{a1}A_a\{\boldsymbol{C}_1^{a'}\}^T}{M_{a1}} \quad \frac{h_{a2}A_a\{\boldsymbol{C}_2^{a'}\}^T}{M_{a2}} \quad \cdots \quad \frac{h_{am}A_a\{\boldsymbol{C}_m^{a'}\}^T}{M_{am}}\right]^T \tag{23}$$

$$\boldsymbol{H}_b = \left[\frac{h_{b1}A_b\{\boldsymbol{C}_1^{b'}\}^T}{M_{b1}} \quad \frac{h_{b2}A_b\{\boldsymbol{C}_2^{b'}\}^T}{M_{b2}} \quad \cdots \quad \frac{h_{bs}A_b\{\boldsymbol{C}_s^{b'}\}^T}{M_{bs}}\right]^T \tag{24}$$

Where $\boldsymbol{C}_n^a$ and $\boldsymbol{C}_n^b$ are row vectors of coupling coefficients matrices $\boldsymbol{C}^a$ and $\boldsymbol{C}^b$; $\boldsymbol{C}_m^{a'}$ and $\boldsymbol{C}_s^{b'}$ are their column vectors. Combining Eqs. (16)-(18), the complex amplitude of sound pressure can be obtained as

$$\boldsymbol{P} = \boldsymbol{P}_p + \boldsymbol{AV} \tag{25}$$

Where $\boldsymbol{P}_p$ is the modal complex amplitude of sound pressure in the uncontrolled case, and

$$\boldsymbol{P}_p = (\boldsymbol{I} + \boldsymbol{Z}_a\boldsymbol{H}_a + \boldsymbol{Z}_b\boldsymbol{H}_b)^{-1}\boldsymbol{Z}_a\boldsymbol{Q}_F \tag{26}$$

$$\boldsymbol{A} = (\boldsymbol{I} + \boldsymbol{Z}_a\boldsymbol{H}_a + \boldsymbol{Z}_b\boldsymbol{H}_b)^{-1}\boldsymbol{Z}_a\boldsymbol{D}_k \tag{27}$$

Where $\boldsymbol{I}$ is an identity matrix. Thus, the acoustic pressure in the enclosure can be expressed as

$$\begin{aligned} p(r,\omega) &= \sum_{n=1}^{N}\psi_n(r)P_n(\omega) = \boldsymbol{\psi}^T\boldsymbol{P} = \boldsymbol{\psi}^T\boldsymbol{P}_p + \boldsymbol{\psi}^T\boldsymbol{AV} \\ &= p_p(r,\omega) + \boldsymbol{\psi}^T\boldsymbol{AV} \end{aligned} \tag{28}$$

Here $p_p(\boldsymbol{r}, \omega)$ is the sound pressure in the cavity before control.

2.2 Cost function

The acoustic potential energy in the enclosure is adopted as the cost function which is used to evaluate the noise level. An alternative is to use R number of sensors (microphones) to perform a local minimization, because a global acoustical potential energy control is impractical. Then, the local acoustical potential energy is used as the cost function and defined by

$$E_p = \frac{1}{4\rho c^2 R}\sum_{i=1}^{R}|p(r_i,\omega)|^2 = \frac{1}{4\rho c^2 R}\boldsymbol{P}^H\boldsymbol{\psi}_R\boldsymbol{\psi}_R^T\boldsymbol{P} \tag{29}$$

Where the superscript T and H denote the transpose and complex conjugate transpose, respectively. $\boldsymbol{\psi}_R$ is a matrix of mode shapes at the R microphone locations. Substituting Eq. (25) into Eq. (29) then results in a quadratic function expression of control inputs

$$E_p = \boldsymbol{V}^{\boldsymbol{H}}\boldsymbol{aV} + \boldsymbol{V}^{\boldsymbol{H}}\boldsymbol{b} + \boldsymbol{b}^{\boldsymbol{H}}\boldsymbol{V} + \boldsymbol{c} \tag{30}$$

Thus, the optimal values for control voltage and acoustical potential energy are given by

$$\boldsymbol{V}_{opt} = -\boldsymbol{a}^{-1}\boldsymbol{b} \tag{31}$$

$$E_p^{opt} = \boldsymbol{c} - \boldsymbol{b}^H\boldsymbol{a}^{-1}\boldsymbol{b} \tag{32}$$

Where $\boldsymbol{a} = \boldsymbol{A}^H\boldsymbol{\psi}_R\boldsymbol{\psi}_R^T\boldsymbol{A}/4\rho c^2 R$, $\boldsymbol{b} = \boldsymbol{A}^H\boldsymbol{\psi}_R\boldsymbol{\psi}_R^T\boldsymbol{P}_p/4\rho c^2 R$, $\boldsymbol{c} = \boldsymbol{P}_p^H\boldsymbol{\psi}_R\boldsymbol{\psi}_R^T\boldsymbol{P}_p/4\rho c^2 R$.

3. Integrated control system with smart structures

3.1 Local control problem

Firstly, consider the characteristics of the primary acoustic field. Assume that Panel a is excited by a disturbance point force F which is located at (0.3, 0.4) m on the Panel a. The amplitude of the force F is 1 N. Four microphones are used as sensors for monitoring the acoustic pressure, and located at s_1 = (0.8, 1.1, 0.05), s_2 = (0.43, 0.57, 0.5), s_3 = (0.05, 0.05, 0.95), and s_4 = (0.8, 0.05, 0.05) m within the enclosure. Panels a and b with thicknesses of 6 mm are aluminum panels with the material properties of Young's modulus E = 71 GPa, mass density ρ_1 = 2770 kg m^{-3}, and Poisson's ratio υ = 0.33. The modal damping ratios of the panels and the cavity are both assumed to be 0.01, and the time constant (T_a) of the first acoustic mode is taken to be 0.2 s. The sound speed is c = 340 m s^{-1}, and mass density of air is ρ = 1.21 kg m^{-3}. The parameter values of the PZT patch are h_p = 0.254 mm, E_{pzt} = 7.24×10^{10} N m^{-2}, ν_p = 0.3 and d_{31} = 2.74×10^{-10} m V^{-1}, and the PZT patch is 20 mm long and 20 mm wide.

Fig. 2 is the acoustic potential energy in the cavity without control, as a function of the driving frequency. The dB reference for acoustic potential energy is 10^{-12} Joules. Table 1 illustrates the natural frequencies of each uncoupled system. A total of 14 and 13 structural modes of panels a and b, respectively, and 12 acoustic modes are used in the simulations within the frequency range of 0 ~ 350 Hz. As shown in Fig. 2 and Table 1, the high sound pressure response in the cavity is basically caused by the structural-acoustic coupling effects, such as those at coupled nature frequencies 196, 254, and 295 Hz. That is, the structural-acoustic coupling plays a leading role in the sound field. Therefore, the control problem of the noise at a coupled natural frequency is considered as a local control problem. Each local control problem is resolved by a smart structure which includes the controller, the PZT patch actuator, and the sensor (microphone). The smart structure is represented as SS, and the smart structure containing the kth PZT patch is labeled as SS_k. The SS_1, SS_2, SS_3, SS_4, SS_5 and SS_6 are used to control the noise at frequencies 36 Hz (f_1), 148 Hz (f_2),

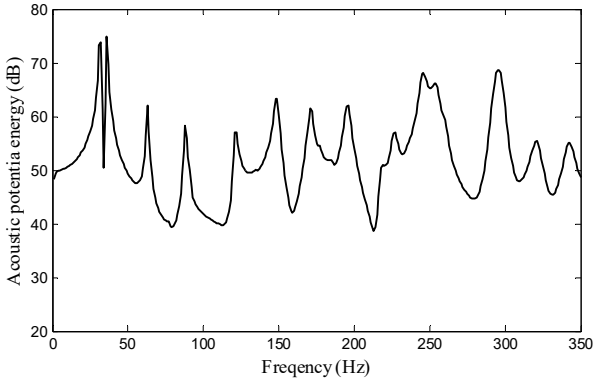

Fig. 2 Acoustic potential energy in the enclosure without control

171 Hz (f_3), 196 Hz (f_4), 254 Hz (f_5) and 295 Hz (f_6), respectively.

The locations of PZT patch actuators for effective control are determined by analyzing the contour plots of the optimal acoustic potential energy level (see Eq. (32)), as shown in Fig. 3. It can be seen that the optimal location regions of the PZT patch in the contour plot for a certain frequency may be more than one. Considering that PZT patches cannot overlap with each other, the optimal positions of the PZT_1 ~ PZT_6 are determined with the coordinate (0.47, 0.35) m, (0.55, 0.65) m, (0.65, 0.7) m, (0.58, 0.74) m, (0.54, 0.43) m and (0.35, 0.42) m on the Panel *a*, respectively, as indicated by the red arrows in Fig 3. The relative locations of all PZT patches applied on Panel *a* are shown in Fig. 1.

Table 1 The modal indices and uncoupled nature frequencies of two panels and enclosure

Panel *a*		Panel *b*		Enclosure	
Mode	*f* (Hz)	Mode	*f* (Hz)	Mode	*f* (Hz)
(1,1)	30.4	(1,1)	34.0	(0,0,0)	0
(1,2)	63.5	(1,2)	77.7	(0,1,0)	147.8
(2,1)	88.5	(2,1)	92.1	(0,0,1)	170.0
(1,3)	118.7	(2,2)	135.8	(1,0,0)	195.9
(2,2)	121.6	(1,3)	150.7	(0,1,1)	225.3
(2,3)	176.8	(3,1)	188.9	(1,1,0)	245.4
(3,1)	185.3	(2,3)	208.8	(1,0,1)	259.3
(1,4)	195.9	(3,2)	232.7	(0,2,0)	295.7
(3,2)	218.4	(1,4)	252.8	(1,1,1)	298.5
(2,4)	254.0	(3,3)	305.6	(0,0,2)	340.0
(3,3)	273.6	(2,4)	310.9	(0,2,1)	341.0
(1,5)	295.2	(4,1)	324.5	(1,2,0)	354.6
(4,1)	320.9	(4,2)	368.2		
(3,4)	350.8				

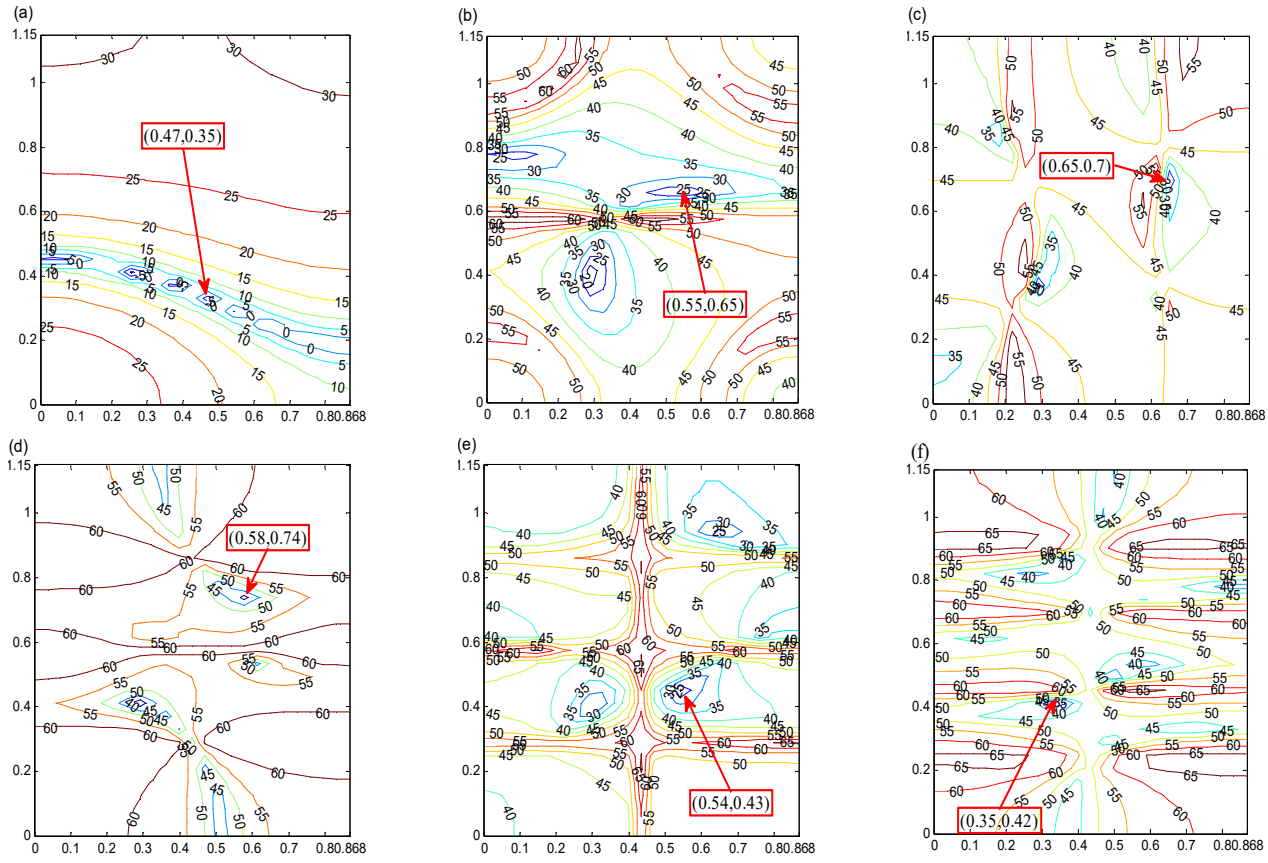

Fig. 3 Contour plots of the optimal acoustic potential energy level. (a) f_1 = 36 Hz; (b) f_2 = 148 Hz; (c) f_3 = 171 Hz; (d) f_4 = 196 Hz; (e) f_5 = 254 Hz; (f) f_6 = 295 Hz

3.2 Smart structure design

The solution of the local problem is implemented by the *SS*. Fig. 4 shows a block diagram of the internal architecture of the controller. The controller consists of several functions such as the *start function*, *blend function*, and *optimal function*. The *start function* defines the operating regime of the *SS*. It is defined by

$$E_{pf_k} \geq T_{f_k} \tag{33}$$

Where E_{pf_k} is the primary acoustic potential energy at the coupled natural frequency, f_k. T_{f_k} is the single-frequency noise threshold. Considering that human ear hearing has different sensitivity at different frequency noises, and according to the relationship between A-weighted sound level and relative sound pressure level, T_{36}, T_{148}, T_{171}, T_{196}, T_{254} and T_{295} are taken as 72 dB, 44 dB, 42 dB, 40 dB, 38 dB and 37 dB, respectively. If the effect of the sound quality is added, T_{f_k} can also be adjusted properly. If the formula (33) is satisfied, the *SS* can start and send binary signal (1) to the upper level organization; or else, the *SS* cannot start and send binary signal (0) to the upper level organization. The switching behavior of the start state is described by a finite state machine, as shown in Fig. 5(a). Another finite state machine is used to describe the operating state of the *SS*. The operating state is controlled by a control instruction from the upper level organization. If the instruction is "1", then the *SS* becomes or stays active; if the instruction is "0", the *SS* becomes or stays inactive. When the operating state switches from "inactive" to "active", the *SS* executes the *initialize function*. Conversely, it executes the *finalize function*. Fig. 5(b) describes the switching behavior of the operating state. Eqs. (27)-(28) indicate that the control effect of sound pressure in the enclosure is related to $\boldsymbol{D}_k$. It reflects the contribution of all PZT actuators/*SS*s to noise suppression. Hence, the *blend function* is defined by $\boldsymbol{D}_k$ in Eq. (22). It can blend the control weights of the controllers into a global output.

The *optimal function* is defined by Eq. (31). The calculation result of the *optimization function* is based on the output of the *blend function*. Therefore, the *optimization function* implements global optimization. It outputs the optimal control voltage for all actuators. Hence, the control system has the control performance of the centralized control. The *output allocation* function block distributes the optimal control voltage V_k to the corresponding PZT$_k$ actuator. The controller also contains an *update function* that updates the internal state variables. It is executed in both operating states.

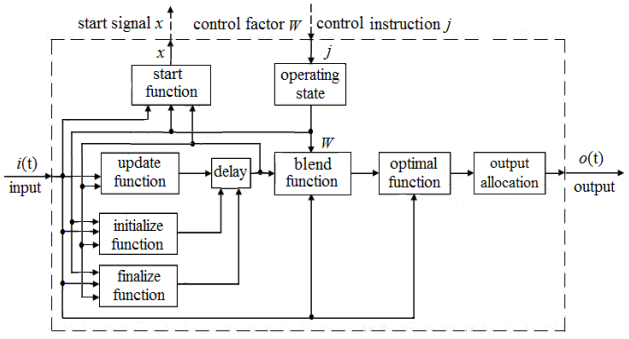

Fig. 4 Internal architecture of a *SS* controller

3.3 Integrated control system

The behavioral relationships among the *SS*s are coordinated by an upper level organization called coordination structure, as shown in Fig. 6. It includes three-step coordination procedure (admission, decision and joint control/cooperation) and two coordination mechanisms (competition and cooperation). When the *SS*s send the start signals (1) to the coordination structure, the coordination structure begins to execute the first procedure: admission. Whether or not to agree to start depends on the admission function which is given by

$$E_{\text{pmax}} \geq T \tag{34}$$

Where E_{pmax} that is calculated by Eq. (29) is the maximum potential energy in the enclosure. T is the noise threshold of the frequency band considered, and it is taken as 50 dB. Only if the formula (34) is satisfied, the *SS* can be started and entered into the next procedure, otherwise the *SS* can be denied entry. If the formula (34) holds, and only one *SS* sends start signal, the coordination structure directly agrees with its activation. If several *SS*s send start signal at the same time, the coordination structure executes the second procedure: decision. That is, the activation of the *SS* is determined by a competition mechanism. The competition mechanism is executed by a decision function which is given by

$$J_{SS_k} = \begin{cases} 1, & y_{k\min} \in Y = \{y_k = |f_k - f_{max}|\} \\ 0, & \text{otherwise} \end{cases} \tag{35}$$

Where f_{max} is the frequency of the maximal acoustic potential energy. The decision function is used in the

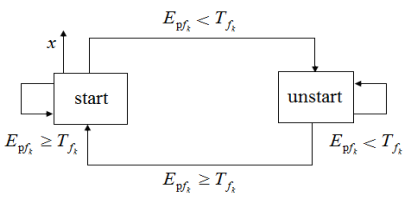

(a) Start state

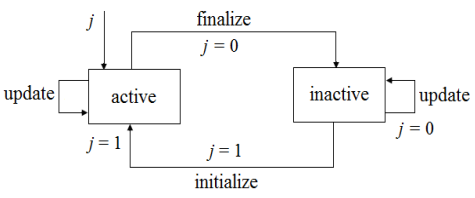

(b) Operating state

Fig. 5 Switching behavior of the *SS*

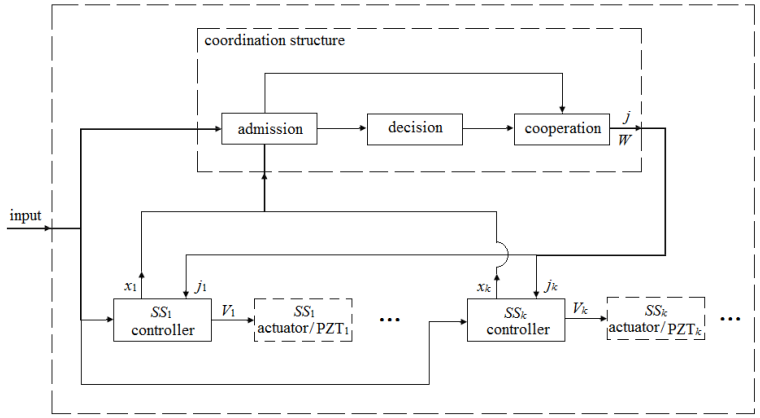

Fig. 6 Framework of the integrated control system

inactivated *SS*s that send start signals. When y_k ($\in Y$) is the minimum $y_{k\min}$, SS_k can be activated. Then the coordination structure begins to implement the third procedure: joint control. If only one *SS* is activated, it receives a positive instruction (1) and corresponding control factor from the coordination structure, and executes the *initialization function*. The rest of the *SS*s receive negative instructions (0) and cannot be activated. If several *SS*s are activated, they need to achieve joint control through cooperation mechanisms. The cooperation mechanism is designed by allocating the corresponding control factors. Considering that PZT's contribution to noise reduction depends on the secondary generalized modal force, $D_{m,k}$, it is defined as control factor. By Eq. (22), $\boldsymbol{D}_k$ can be expressed as

$$\boldsymbol{D}_k = \begin{bmatrix} \frac{h_{a1}}{M_{a1}} & \frac{h_{a1}}{M_{a1}} & \cdots & \frac{h_{a1}}{M_{a1}} \\ \frac{h_{a2}}{M_{a2}} & \frac{h_{a2}}{M_{a2}} & \cdots & \frac{h_{a2}}{M_{a2}} \\ \vdots & \vdots & \ddots & \vdots \\ \frac{h_{am}}{M_{am}} & \frac{h_{am}}{M_{am}} & \cdots & \frac{h_{am}}{M_{am}} \end{bmatrix} \bullet * \begin{bmatrix} D_{1,1} & D_{1,2} & \cdots & D_{1,k} \\ D_{2,1} & D_{2,2} & \cdots & D_{2,k} \\ \vdots & \vdots & \ddots & \vdots \\ D_{m,1} & D_{m,2} & \cdots & D_{m,k} \end{bmatrix} \tag{36}$$

Where "$\bullet *$" means dot product. The column vectors in the first matrix on the right side of the equation are all the same, and each column is represented as $\boldsymbol{D}_{hm}$, that is $\boldsymbol{D}_{hm} = [h_{a1}/M_{a1},\ h_{a2}/M_{a2},\ \ldots,\ h_{am}/M_{am}]^{\mathrm{T}}$. The number of column vectors is the same as the number of PZT actuators. Each column vector in the second matrix on the right side of the equation corresponds to a PZT actuator. When the coordinate (x, y) of the centre of a PZT patch on the Panel a is determined, $\varphi_m(\sigma_a)$ is a constant. It can be seen through the expression of the secondary generalized modal force, $D_{m,k} = \frac{(h_a+h_p)E_{\mathrm{pzt}}d_{31}}{(1-v_p)}\int_{A_a}\varphi_m(\sigma_a)\,(\nabla^2\chi_k)dA$, that $D_{m,k}$ is a constant. Therefore, the constant vector, $\boldsymbol{W}_k = [D_{1,k},\ D_{2,k},\ \ldots,\ D_{m,k}]^{\mathrm{T}}$, is extracted from $\boldsymbol{D}_k$ and stored in the *cooperation* function block of the coordination structure. The cooperation of the *SS*s are realized through the *blend function*.

Before the control factor $D_{m,k}$ is extracted from the blend function D_k, the optimization function in the *SS* (Eq. (31)) is global optimization, that is, the *SS* performs centralized control. In Eq. (31), the expression of the optimal control voltage contains $\boldsymbol{A}$, $\boldsymbol{A}$ contains blend function D_k, and D_k contains the control factor $D_{m,k}$. The magnitude of the control factor $D_{m,k}$ mainly depends on the position of the PZT actuator. Because the position of the PZT actuators is different, the internal functions of the *SS*s are different. This makes the installation, maintenance and interchange of the *SS*s difficult. Considering that the control factors play a key role in the noise control of the *SS*, they are extracted from the blend function and stored in the upper control unit (coordination structure). According to the real-time changes of sound field, the control factors are allocated to the activated *SS*s through the coordination structure. On the one hand, this design method retains the advantages of centralized control of the control system, on the other hand, it eliminates the main differences in the internal composition of *SS*, and provides support for the decentralized control. At the same time, this design method also solves the coupling problem between *SS*s, which is often a difficult problem to solve.

For the ease of installation and maintenance of the system, the internal design of each *SS* is basically the same. The internal functions and function blocks of each *SS* are the same except for the start function. Simply changing the threshold T_{f_k} in the start function allows the *SS*s to be interchanged. Each *SS* is an independent control system that can operate independently. In addition, when a new *SS* is added, the adjustment of the control system can be completed only by adding corresponding control factors of the new *SS* to the coordination structure. Through the flexible docking of control factors and joint functions, the centralized control of the system is realized. Meantime the conflict and cooperation among *SS*s are resolved. Using the bottom-up launch application and the top-down activation response method enables the system to implement intelligent logical judgment. The system can receive all the sensor signals and use it to generate global optimization control voltage, so that the system has the characteristics of

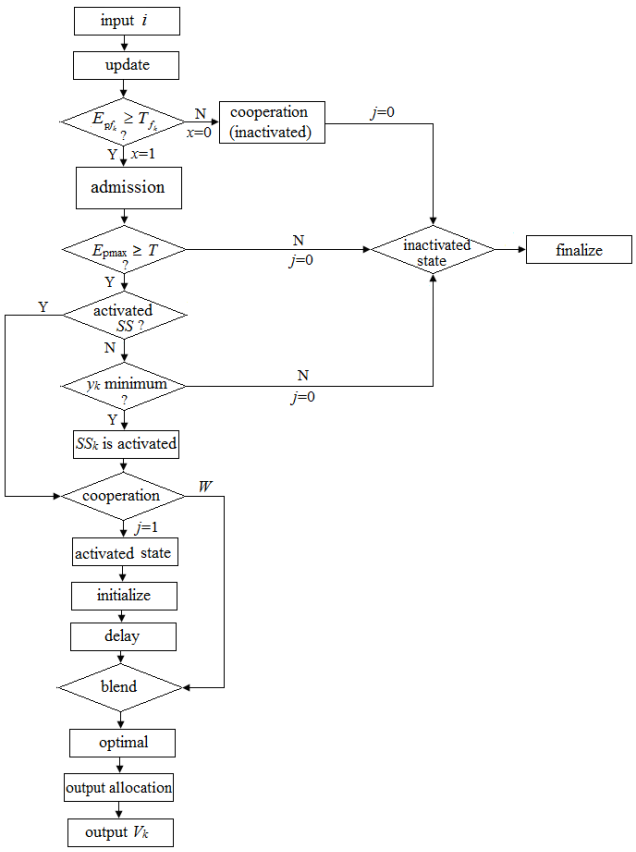

Fig. 7 Control flow of the integrated control system

high control performance of the centralized control. The system adopts modular design, so that the system has the characteristics of high reliability, high fault tolerance and easy installation and maintenance of the decentralized control. Therefore, an integrated control system based on *SS* is established for active control of vibration noise, as shown in Fig. 6. x_1, …, x_k and j_1, …, j_k correspond to the start signals and control instructions of SS_1, …, SS_k, respectively. The control flow is shown in Fig. 7.

4. Results and discussion

The validity of the model is verified. The model and parameters set in this paper are exactly the same as those in the publication (Jin *et al*. 2009). The primary excitation is an external perturbing noise source, and a PZT actuator is arranged on Panel *a* to control the sound field in the enclosure. The sound pressure responses obtained by the two modeling methods are consistent, except for some differences in the peak values of the two-order primary potential energy on the left side of the graph, as shown in Fig. 8. Therefore, the effectiveness of the modeling method in this paper is verified.

The advantages of the integrated control system are discussed. To illustrate the ease of installation and maintenance of the system, assume that SS_6 is not designed. From Fig. 2 and the *start function*, the following inequality can be obtained: $E_{p1(36)}$ = 76.24 dB ≥ T_{36} = 72 dB, $E_{p2(148)}$ = 64.8 dB ≥ T_{148} = 44 dB, $E_{p3(171)}$ = 63.45 dB ≥ T_{171} = 42 dB, $E_{p4(196)}$ = 66.26 dB ≥ T_{196} = 40 dB, $E_{p5(254)}$ = 69.69 dB ≥ T_{254} = 38 dB. Thus, all *SS*s meet the start conditions and send the start signals to the coordinated structure. It can be seen from Fig. 2 and the *admission function* that E_{pmax} = 76 dB ≥ T = 50 dB satisfies the formula (34). According to the *decision function* in the coordination structure, y_1 (= |36-36| = 0) in the set of Y is the minimum. Hence, the SS_1 can receive a positive instruction, j = 1, and the control factor vector, $\boldsymbol{W}_1$ = [0.1348, 0.173, -0.035, 0.0872, -0.0449, -0.0227, -0.1257, -0.0611, -0.1613, 0.0159, -0.0813, -0.1656, 0.0677, 0.057]^T, from the coordination structure. That is, the SS_1 is activated. The other *SS*s can receive the negative instructions, j = 0, and remain inactive. The output of the *blend function* $\boldsymbol{D}_k$ is the result of the dot multiplication of $\boldsymbol{D}_{hm}$ and $\boldsymbol{W}_1$. The optimal control voltage, V_1 = -7.6673 + 4.905i, is obtained by the *optimal function* and applied to the PZT_1 actuator. The maximum potential energy in the enclosure is about 58 dB at 197 Hz after the SS_1 control, as shown in Fig. 9. In the next signal update cycle, the SS_1 continues to send the start signal, and the coordination structure directly agrees that it stays active. The rest of the *SS*s that send the start signal use the *decision function* to decide which one is activated. Because y_4 (= |197-196| = 1) is the minimum in the set of Y, the SS_4 is activated. Hence, the control factor matrix, [$\boldsymbol{W}_1$, $\boldsymbol{W}_4$] = [0.1348, 0.173, -0.035, 0.0872, -0.0449, -0.0227, -0.1257, -0.0611, -0.1613, 0.0159, -0.0813, -0.1656, 0.0677, 0.057; 0.1378, -0.12, -0.1389, -0.0332, 0.121, 0.0335, 0.0023, 0.149, -0.002, -0.1502, -0.0006, -0.0966, 0.1366, 0.0025]^T, and positive instruction, j = 1, from the coordination structure are sent simultaneously to the SS_1

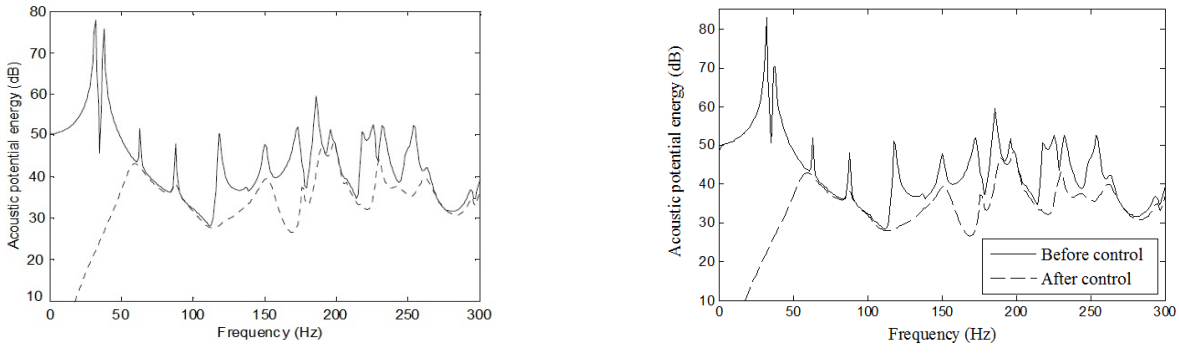

(a) Modeling method in the publication (Jin *et al*. 2009)

(b) Modeling method in this paper

Fig. 8 Comparison of acoustic potential energy before and after control

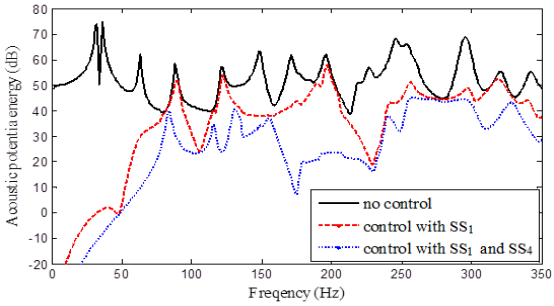

Fig. 9 Control performance of the integrated control system under normal condition

and SS_4. The output of the *blend function* of each *SS* is [$\boldsymbol{D}_{hm}$•∗$\boldsymbol{W}_1$, $\boldsymbol{D}_{hm}$•∗$\boldsymbol{W}_4$]. The output of the *optimal function* is [V_1; V_4] = [-5.1593 + 1.7906i; -2.9424 + 2.4432i]. V_1 and V_4 are allocated to the PZT_1 and PZT_4 respectively through the *output allocation* function block. The maximum potential energy in the enclosure is about 45 dB after the SS_1 and SS_4 joint control, as shown in Fig. 9. Due to E_{pmax} = 45 < T = 50, the start signals sent by the inactivated *SS*s are not processed by the coordination structure. The integrated control system begins to run smoothly and achieves high control performance of the centralized control.

Can the control system run stably and maintain good control performance when one or several *SS*s fail? Assume that the SS_1 and SS_4 have failed and cannot send start signal. Thus, y_2 (= |148-36| = 112) is the minimum in the Y, and the SS_2 is activated. After the SS_2 control, the maximum acoustic potential energy in the enclosure is about 63 dB at 258 Hz, as shown in Fig. 10. In the second round of signal update, since y_5 (= |254-258| = 4) is the minimum in the Y, the SS_5 is also activated. After the joint control of the two *SS*s, the maximum potential energy at 298 Hz is about 54 dB (Fig. 10). Due to E_{pmax} = 54 ≥ T = 50 and lack of competition, the SS_3 is directly activated by the coordination structure. Hence, the SS_2, SS_5 and SS_3 can receive positive instruction, j = 1, and control factor matrix, [$\boldsymbol{W}_2$, $\boldsymbol{W}_5$, $\boldsymbol{W}_3$] = [0.8941, -0.3638, -0.7289, -0.746, 0.2966, 0.6082, -0.2999, 0.6674, 0.122, -0.5441, 0.2502, 0.4745, 0.9733, -0.2238; 0.8555, 0.6602, -0.6404, -0.3461, -0.4942, 0.2591, -0.3761, -0.9272, -0.2902, 0.6941, 0.1521, -0.3694, 0.922, 0.4076; 0.6687, -0.4479, -0.9422, -0.3687, 0.6311, 0.5196, 0.659, 0.6948, -0.4414, -0.9791, -0.3634, -0.0966, 0.0136, 0.6848]^T, simultaneously. The output of the *blend function* of each *SS* is [$\boldsymbol{D}_{hm}$•∗$\boldsymbol{W}_2$, $\boldsymbol{D}_{hm}$•∗$\boldsymbol{W}_5$, $\boldsymbol{D}_{hm}$•∗$\boldsymbol{W}_3$]. The optimized control voltage, [V_2; V_5; V_3] = [0.3982 - 0.0744i; 1.8647 + 4.2864i; -3.5442 - 2.8872i], is obtained through the *optimization function*. The control voltage V_2, V_5 and V_3 are applied to the PZT_2, PZT_5 and PZT_3 by the *output allocation* function block, respectively. After the three *SS*s are jointly controlled, the acoustic potential energy in the enclosure is greatly reduced. The maximum acoustic potential energy is only about 33 dB at 139 Hz (see Fig. 10), which ensures the stability and control performance of the control system. It is also found that, although the common control effects of the SS_2 and SS_5 are less than the SS_1 and SS_4, good control performance can be obtained by activating more *SS*s. That is, the integrated control system with redundant *SS*s can tolerate one or more *SS*s failures. Hence, the integrated control has higher reliability and fault tolerance than the centralized control.

In addition, after the joint control of the SS_2 and SS_5, it is found that the maximum acoustic energy potential at 298 Hz is mainly caused by the resonance frequency of 295 Hz (see Figs. 11 and 2). Therefore, the noise at 298 Hz can be solved by adding a new *SS* (SS_6). The optimal position of the SS_6 is located at (0.35, 0.42) m on the Panel *a*, as shown in Fig. 3(f). Thus, the control factor vector (W_6 = [0.8699, 0.7148, 0.5208, -0.2824, 0.428, -0.1691, -0.558, -0.9469, -0.4586, -0.567, 0.1812, -0.4958, -0.8549, 0.6075]^T) is determined. Only need to add the corresponding control factor (W_6) of the SS_6 in the cooperation function of the coordination structure and set the *start function*, $E_{p6(295)} \geq T_{295}$ = 37 dB, in the SS_6, then the SS_6 can be easily installed into the control system. Since $E_{p6(295)}$ = 70.09 dB ≥ T_{295} = 37 dB, the SS_6 satisfies the start condition, and y_6 (= |295-298| = 3) is the minimum in the set Y, the SS_6 is activated instead of the SS_3. The optimized control voltage V_2 (= -1.6443 + 1.1888i), V_5 = (2.6337 - 3.8144i) and V_6 = (-5.5779 + 2.8537i) are applied to the PZT_2, PZT_5 and PZT_6 by the *output allocation* function block, respectively. After the SS_2, SS_5 and SS_6 jointly control, the maximum acoustic potential energy in the enclosure is only about 30 dB at 269 Hz, as shown in Fig. 11. Thus, the system has the better control performance after the SS_6 instead of the SS_3. Alternatively, the SS_3 can also be removed from the system and easily remodeled to the SS_6. Therefore, the *SS*s can easily be added or removed from the integrated control system to achieve

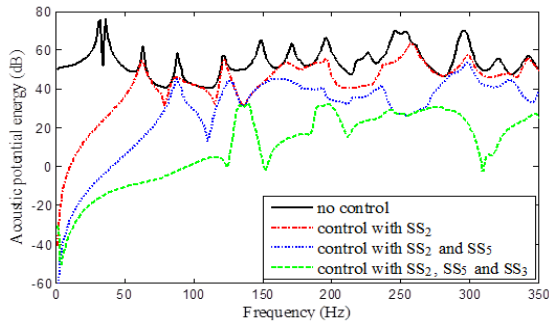

Fig. 10 Control effect of the integrated control system in the case of the SS_1 and SS_4 failure

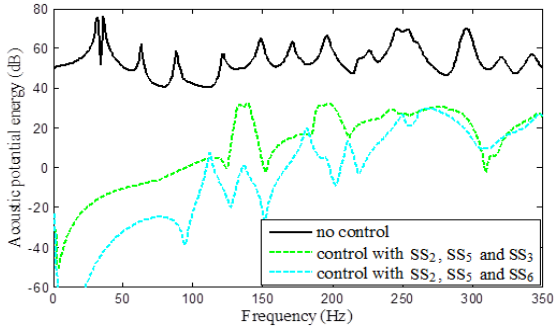

Fig. 11 Comparison of control effects before and after adding the SS_6 to replace the SS_3

better control performance, that is, the system has the characteristics of easy installation and maintenance of the decentralized control.

The above three cases show that the integrated control system has the advantages of centralized and decentralized control. The following further analyzes the characteristics of the control system from the perspective of algorithms. The control system adopts quadratic objective function optimization algorithm. The optimal control voltage is calculated by Eq. (31), that is, the optimization function in the *SS* adopts the global optimization method, thus it has the characteristic of centralized control. In Eq. (31), $\boldsymbol{V}_{opt} = -(\boldsymbol{A}^H\boldsymbol{\psi}_R\boldsymbol{\psi}_R^T\boldsymbol{A}/4\rho c^2R)^{-1}\left(\boldsymbol{A}^H\boldsymbol{\psi}_R\boldsymbol{\psi}_R^T\boldsymbol{P}_p/4\rho c^2R\right)$, the modal complex amplitude of sound pressure $\boldsymbol{P}_{\mathrm{p}}$ comes from the primary sound field, that is, $\boldsymbol{P}_{\mathrm{p}}$ is obtained by processing the signal collected by the microphone; R is the number of microphones. When the microphone position is fixed, the acoustic mode shape function at R microphones is a constant matrix (12 rows × 4 columns). Therefore, except for $\boldsymbol{P}_{\mathrm{p}}$ and A, the other parameters are constant. In the expressions of $\boldsymbol{Z}_a$ (Eq. (19)) and $\boldsymbol{Z}_b$ (Eq. (20)) in Eq. (27), $\boldsymbol{A} = (\boldsymbol{I} + \boldsymbol{Z}_a\boldsymbol{H}_a + \boldsymbol{Z}_b\boldsymbol{H}_b)^{-1}\boldsymbol{Z}_a\boldsymbol{D}_k$, except that h_n is related to primary excitation (primary sound field), the other parameters are determined by the properties of the acoustic enclosure and structure. Similarly, in the expressions of $\boldsymbol{H}_a$ (Eq. (23)) and $\boldsymbol{H}_b$ (Eq. (24)), except that h_{am} and h_{bs} are related to the primary sound field, the other parameters are also determined by the properties of the acoustic enclosure and structure. Before the control factor is extracted, in the expression of $\boldsymbol{D}_k$ (Eq. (22)), h_{am} is related to the primary sound field, and $\boldsymbol{M}_{am}$ is related to the structural properties of Plate a. However, the control factor (generalized mode secondary force) is related to the location of PZT actuator, so the $\boldsymbol{D}_k$ functions in *SS*s are different. In addition, the control factor is considered as the weight of the *SS* to the noise control, which is extracted and stored in the upper coordination unit, so as to ensure the consistency of the functions in the *SS*s and lay the foundation for the decentralized control. In the above analysis, all the parameters related to the properties of the acoustic enclosure and the structure can be calculated before control, that is, these parameters in different *SS*s are the same. In addition, the sound signals (primary sound field) input into the *SS*s through the microphones are also the same. Therefore, this design idea, combined with the multi smart structure framework, skillfully integrates the advantages of centralized control and decentralized control.

5. Conclusions

The *SS*s are integrated through an intelligent framework. Broadly speaking, the *SS* with modular design is a relatively independent control system. In terms of form, because there is no centralized control center, the discretely distributed *SS* forms a decentralized control. The relationship between *SS*s is regulated by the upper coordination unit. The control factors (the different weights of the *SS* for noise control) in each *SS* are extracted to the upper coordination unit, so that the internal structure of each *SS* is basically the same. According to the real-time change of sound field, the control factors are re-allocated to the *SS*s by using the upper coordination unit, thus forming the centralized control in algorithm.

- The *SS* has certain autonomy and independence, and its internal composition is basically the same, thus the control system has the characteristics of high reliability, easy installation and maintenance of decentralized control. Meanwhile, the different combinations of the control factors are used to achieve the centralized control of the control system, which obtains better control performance than the pure decentralized control. That is, the control system integrates the advantages of decentralized control and centralized control.
- The coupling problem among control units in decentralized control is a difficult problem. The extraction and redistribution of the control factors ingeniously solve the coupling problem among various *SS*s. At the same time, the extraction of control factors makes the internal functions of each *SS* basically consistent. This is also a major feature of this paper in the design of the control system.

For the noise intelligent control method proposed in this paper, only the simulation research has been carried out, and its limitations are mainly manifested in the following aspects: 1) The assumptions and preconditions of the simulation model are relatively ideal, and there is a certain deviation between the actual sound field and the analytical solution obtained by the simulation calculation; 2) The calculation amount of the algorithm and the time used by the algorithm are not considered in the simulation research. It is not yet known whether hardware such as DSP chips can meet the computing requirements in experiments or practical applications; 3) The simulation results and the hypotheses in the discussion are artificial factors added to the simulation, which are not real reality. However, the experiment may be disturbed by various factors, and the stability of the system needs further verification. The next research goal is to verify the method in this paper through experiment.

Acknowledgments

This work was supported by the Basic Public Welfare Research Project of Zhejiang Province, China (Grant No. LGG18E050019); A Project Supported by Scientific Research Fund of Zhejiang Provincial Education Department, China (Grant No. Y201737638); and the Natural Science Foundation of Ningbo, China (Grant No. 2019A610160).

References

Algermissen, S. and Monner, H.P. (2017), "On the stability of decentralized AVC ASAC for large-scale structures", *J. Intel. Mater. Syst. Struct.*, **28**(16), 2255-2264.

https://doi.org/10.1177/1045389X16682843
Aridogan, U. and Basdogan, I. (2015), "A review of active vibration and noise suppression of plate-like structures with piezoelectric transducers", *J. Intel. Mat. Syst. Struct.*, **26**(12), 1455-1476. https://doi.org/10.1177/1045389X15585896
Alujevi, N., Gardonio, P. and Frampton, K.D. (2008), "Smart double panel with decentralized active damping units for the control of sound transmission", *AIAA J.*, **46**, 1463-1475.
Bagha, A.K. and Modak, S.V. (2017), "Feedback control strategies for active control of noise inside a 3-D vibro-acoustic cavity", *Smart Struct. Syst., Int. J.*, **20**(3), 273-283. https://doi.org/10.12989/sss.2017.20.3.273
Baumann, O.N. and Elliott, S.J. (2007), "Global optimization of distributed output feedback controllers", *J. Acoust. Soc. Am.*, **122**(3), 1587-1594. https://doi.org/10.1121/1.2756796
Engels, W.P. and Elliott, S.J. (2008), "Optimal centralized and decentralized velocity feedback control on a beam", *Smart Mater. Struct.*, **17**(2), 1-10. https://doi.org/10.1088/0964-1726/17/2/025009
Engels, W.P., Baumann, O.N. and Elliott, S.J. (2006), "Centralized and decentralized control of structural vibration and sound radiation", *J. Acoust. Soc. Am.*, **119**(3), 1487-1495. https://doi.org/10.1121/1.2163270
Frampton, K.D. (2006), "Vibro-acoustic control with a distributed sensor network", *J. Acoust. Soc. Am.*, **119**(4), 2170-2177. https://doi.org/10.1121/1.2178704
Frampton, K.D., Baumann O.N. and Gardonio P. (2010), "A comparison of decentralized, distributed, and centralized vibro-acoustic control", *J. Acoust. Soc. Am.*, **128(**5), 2798-2806. https://doi.org/10.1121/1.3183369
Gardonio, P., Bianchi, E. and Elliott, S.J. (2004a), "Smart panel with multiple decentralized units for the control of sound transmission, Part 1: theoretical predictions", *J. Sound Vib.*, **274**(1-2), 163-192. https://doi.org/10.1016/j.jsv.2003.05.004
Gardonio, P., Bianchi, E. and Elliott, S.J. (2004b), "Smart panel with multiple decentralized units for the control of sound transmission, Part II: design of the decentralized control units", *J. Sound Vib.*, **274**, 193-213. https://doi.org/10.1016/j.jsv.2003.05.007
Hasheminejad, S.M. and Shakeri, R. (2017), "Active transient acousto-structural response control of a smart cavity-coupled circular plate system", *Arch. Acoust.*, **42**(2), 273-286. https://doi.org/10.1515/aoa-2017-0030
Hasheminejad, S.M., Hakimi, A. and Keshavarzpour, H. (2018), "Broadband sound transmission loss enhancement of an arbitrary-thick hybrid smart composite plate using multi-objective particle swarm optimization–based active control", *J. Intel. Mat. Syst. Struct.*, **29**(8), 1724-1747. https://doi.org/10.1177/1045389X17754257
Jin, G.Y., Liu, Z.G. and Yang, T.J. (2009), "Active control of sound transmission into an acoustic cavity surrounded by more than one flexible plate", *Noise Control Eng. J.*, **57**(3), 210-220.

Landau, I.D., Alma, M., Constantinescu, A., Martinez, J.J. and Noë, M. (2011), "Adaptive regulation-Rejection of unknown multiple narrow band disturbances (a review on algorithms and applications)", *Control Eng. Pract.*, **19**(10), 1168-1181. https://doi.org/10.1016/j.conengprac.2011.06.005
Larbi, W., Deü, J.F. and Ohayon, R. (2012), "Finite element formulation of smart piezoelectric composite plates coupled with acoustic fluid", *Compos. Struct.*, **94**(2), 501-509. https://doi.org/10.1016/j.compstruct.2011.08.010
Quaegebeur, N., Micheau, P. and Berry, A. (2009), "Decentralized harmonic control of sound radiation and transmission by a plate using a virtual impedance approach", *J. Acoust. Soc. Am.*, **125**(5), 2978-2986. https://doi.org/10.1121/1.3106124
Ringwelski, S. and Gabbert, U. (2010), "Modeling of a fluid-loaded smart shell structure for active noise and vibration control using a coupled finite element-boundary element approach", *Smart Mater. Struct.*, **19**(10), 1-13. https://doi.org/10.1088/0964-1726/19/10/105009
Schiller, N.H. and Cabell, R.H. (2010), "Decentralized control of sound radiation using iterative loop recovery", *J. Acoust. Soc. Am.*, **128**(4), 1729-1737. https://doi.org/10.1121/1.3479541
Yuan, M., Qiu, J.H., Ji, H.L., Zhou, W. and Ohayon, R. (2015), "Active control of sound transmission using a hybrid blind decentralized control approach", *J. Vib. Control*, **21**(13), 2661-2684. https://doi.org/10.1177/1077546313514758

HJ